ISSN 1075-7015, Geology of Ore Deposits, 2024, Vol. 66, No. 7, pp. 982–995. © Pleiades Publishing, Ltd., 2024.
Russian Text © The Author(s), 2023, published in Zapiski Rossiiskogo Mineralogicheskogo Obshchestva, 2023, No. 2, pp. 60–79.

MINERALS AND MINERAL PARAGENESES

Lead Phosphates (Pyromorphite and Phosphohedyphane) from the Oxidation Zone of Baryte–Lead Ores in the Ushkatyn-III Deposit, Central Kazakhstan

A. I. Brusnitsyn[a], *, E. N. Perova[a], E. S. Loginov[a], N. V. Platonova[b], **, and L. A. Panova[b]

[a] *Department of Mineralogy, St. Petersburg State University, St. Petersburg, 199115 Russia*
[b] *Research Center for X-ray Diffraction Studies, St. Petersburg State University, St. Petersburg, 199155 Russia*
**e-mail: a.brusnitsin@spbu.ru*
***e-mail: natalia.platonova@spbu.ru*

Received November 7, 2022; revised December 8, 2022; accepted December 14, 2022

Abstract—The paper describes Ca–Pb phosphates—pyromorphite and phosphohedyphane—from the oxidation zone of barite–lead (calcite–barite–galena) ores of the Ushkatyn-III deposit in Central Kazakhstan. Both minerals occur equally frequently within the deposit. Lead phosphates coexist with ore minerals unaltered in the subsurface setting (galena, pyrite, barite, calcite, rhodochrosite, chamosite, etc.), and minerals of highly oxidized ores (cerussite, montmorillonite, kaolinite, goethite, etc.). As the processes of supergene processes develop (during the transition from weakly to highly oxidized ores), the compositions of newly formed phosphates change regularly in the following consequence: phosphohedyphane → rhythmically zonal Ca–Pb phosphate → pyromorphite. At the same time, the habit of mineral crystals changes from dipyramidal-prismatic through elongated prismatic (barrel-shaped) to pinacoidal-prismatic (short-columnar). Crystallization of pyromorphite is possible already at very low contents of lead, phosphorus and chlorine in the solution. The main source of chlorine is groundwater; phosphorus is coming from the organic matter of the soil cover overlying ore-bearing deposits. The features of the chemical composition and crystal structure of Ca–Pb phosphates, as well as the nature of their assemblages, suggest the presence of a discontinuity in isomorphic miscibility in the following series: pyromorphite–phosphohedyphane and phosphohedyphane–chlorapatite.

Keywords: lead phosphates, pyromorphite, phosphohedyphane, oxidation zone, barite–lead ores, Ushkatyn-III deposit, Central Kazakhstan

DOI: 10.1134/S1075701524700107

INTRODUCTION

The Pb phosphates from the apatite supergroup—pyromorphite $Pb_5(PO_4)_3Cl$ and phosphohedyphane $Ca_2Pb_3(PO_4)_3Cl$ are common minerals of the oxidation zones of Pb ores. Pyromorphite was discovered as early as 1813 in deposits near Mt. Zschopau in the Ore Mountains, Germany (Hausmann, 1813; Pasero et al., 2010) and has since been discovered at many other ore occurrences. Phosphohedyphane was approved as a new mineral in 2006. It was found in oxidized Cu–Pb–Ag ores of the Capitana deposits in the Atacama Desert, Chile (Kampf et al., 2006). Moreover, the authors of this discovery noted that lead phosphates, the chemical composition of which corresponds to phosphohedyphane, were known long before 2006. The revision of a large amount of data that had been published by that time showed that "pyromorphite" and "calcium pyromorphite" in about 20% of cases should be called "phosphohedyphane" in a modern context. Thus, it became obvious that phosphohedyphane, as well as pyromorphite, is not a rare mineral. The subsequent studies confirm this fact (see, for example, Birch and Mills, 2007; Jirasek et al., 2020; Ondrejka et al., 2020; and references therein).

However, despite the widespread occurrence of Ca–Pb phosphates, each new find is noteworthy because it allows us to clarify the mineralogy and formation conditions of hypergene lead ores. In this respect, the well-known Ushkatyn-III deposit in the Atasu district of Central Kazakhstan, which combines shoots of iron, manganese and barite–lead ores and their oxidation products, is no exception. This deposit is described in many publications (see Kayupova, 1974; Buzmakov et al., 1975; Mitryaeva, 1979; Rozhnov, 1982; Kalinin, 1985; Skripchenko, 1989; Varentsov et al., 1993; Brusnitsyn et al., 2021a, 2021b, 2022a; and references therein). At the same time, information on the mineralogy of its oxidation zone is not yet sufficient. Nevertheless, virtually all previous researchers mentioned the occurrence of pyromorph-

ite, as one of the main ore lead minerals. Phosphohedyphane was also mentioned (I.V. Pekov, oral communication). However, no specific information about these minerals was provided. Our work aims at filling these gaps. In the course of a comprehensive study of the Ushkatyn-III deposit, new data were obtained on the mineralogy of the oxidation zone of barite–lead ores, including pyromorphite and phosphohedyphane: features of their morphology, mineral assemblages, chemical composition, sequence and conditions of crystallization. A review of mineralogy of oxidized ores is presented in our previous publication (Brysnitsyn et al., 2022b). The present paper is devoted to Pb phosphates.

GEOLOGICAL SETTING OF THE DEPOSIT

The Ushkatyn-III deposit is located 300 km southwest of Karaganda, 15 km northeast of the village of Zhairem. It was discovered in 1962 and has been developed since 1982. The deposit is complex: hydrothermal barite–lead ores and weakly metamorphosed hydrothermal–sedimentary Mn and Fe ores are present in different parts of the carbonate sequence.

The deposit is confined to a paleorift structure filled with Upper Devonian–Lower Carboniferous terrigenous–siliceous–carbonate sedimentary rocks. Within the deposit, red sandstones and siltstones pass from northeast to southwest to reef organogenic-algal limestones and products of their disintegration (calcareous siltstones, sandstones, and sedimentary breccias) and further layered organogenic–detrital limestones.

The reef limestones localize pockety-net and vein-disseminated barite–lead (barite-galena) mineralization, obviously superimposed on the host limestones. The organogenic–detrital limestones host a series of beds (from 5 to 14 in different sections) of iron (hematite) and manganese (hausmannite and braunite) ores syngenetic with the host carbonate deposits.

The Mesozoic–Cenozoic lateritic weathering crust of linear–planar type is developed within the deposit (Kalinin, 1985; *Atlas* ..., 2004; Zhairemsky GOK, 2015). Its average thickness ranges from 30 to 50 m, reaching 100–120 m in the fault zones and up to 220 m in single cases. The weathering products are medium gravel-pelitic-sized loose siliceous-clay deposits of a characteristic brown-yellow color. The primary ore-bearing limestones almost completely lost their lithological features. One can observe only rare "shadow" relics of the original layered-banded texture. Manganese and iron ores in the oxidation zone are replaced by Fe^{3+} and Mn^{3+}/Mn^{4+} oxides—goethite, pyrolusite, vernadite, manganite, coronadite, lithiophorite, and cryptomelane. Cerussite, Pb phosphates, and other minerals occur in oxidized barite–lead ores.

MATERIALS AND METHODS

Research Materials

Samples for our research were collected by the authors in 2016–2019 in the northeastern part of the Ushkatyn-III open pit, where the initial hydrothermal ores and the related oxidation zone crop out to the fullest extent possible. In addition, some samples were taken at the ore stockpile of AO Zhairemsky GOK. Mineralogical studies and thermodynamic calculations were carried out at the Department of Mineralogy and Resource Centers of St. Petersburg State University (SPbSU). In total, more than ten samples of oxidized ores containing phosphate mineralization were studied.

Mineralogical Study of Samples

The complex of traditional methods of studying the matter was used: optical microscopy with transmitted and reflected light modes, X-ray phase analysis, and scanning electron microscopy with energy dispersive X-ray spectroscopy.

The primary mineral diagnostics was carried out at the Department of Mineralogy of SPbSU using a Leica DM2500P optical microscope. The study of polished thin-sections by electron microscopy was carried out at two SPbSU two resource centers (RCs): "Microscopy and Microanalysis" and "Geomodel". The diagnosis of minerals was performed at the "Microscopy and Microanalysis" RC on a Hitachi TM 3000 scanning electron microscope (SEM), equipped with an OXFORD attachment for energy-dispersive microanalysis. The images of bulk microsamples were taken on a QUANTA 200 3D SEM (FIA, Netherlands). Quantitative chemical analysis of minerals was carried out in at the "Geomodel" RC. The analyses were performed on a Hitachi S-3400N scanning electron microscope equipped with an attachment for energy-dispersive microanalysis (Oxford Instruments AzTec Energy X-Max 20). The spectra were recorded at an accelerating voltage of 20 kV, a current of 2 nA, and an exposure time of 60 s. Natural and synthetic compounds were used as standards. The analysts were A.I. Brusnitsyn, E.S. Loginov, S.Y. Yanson, and N.S. Vlasenko.

Powder X-ray phase analyses were performed at the "X-ray Diffraction Methods of Research" RC. There were two directions of research. The first one is diagnostics of minerals on a Rigaku Mini Flex II X-ray diffractometer with Cu$K\alpha$ radiation. Diffractograms of samples were recorded in the range of 2θ angles from 5° to 60° at a rate of °2θ/min. The analysts were A.I. Brusnitsyn, E.S. Loginov, N.V. Platonova, and L.A. Panova. The second direction is the use of the Rietveld method to estimate the distribution of Pb and Ca cations at different positions in the crystal structure of phosphates. For this purpose, one of the samples (Ush-403) was studied on an Ultima IV diffractometer

with Cu$K\alpha$ radiation in the range of 2θ angles from 5° to 125°, imaging rate of 0.125 °2θ/min. The data obtained were processed using Topas 5.0 (Bruker AXS (2014) Topas 5.0: General profile and structure analysis software for powder diffraction data. Karlsruhe, Germany). Structural data from the ICSD (Inorganic Crystal Structure Database 2021) for Ca-pyromorphite (ICSD 201724, Miyake et. al., 1986) and for phosphogediphane (ICSD 156171, Kampf et al., 2006) were used as starting structural models for clarification by the Rietveld method. The analyst was N.V. Platonova.

Calculations of Mineral Equilibriums

Physicochemical diagrams were constructed using the Geochemist`s Workbench Essentials (GWB) 6.0 software, which includes the thermodynamic database thermo.dat (Bethke, 1999; https://www.gwb.com/essentials.php). Calculations were performed for T = 25°C, P = 1 bar, and a wide range of Eh, Ph, and contents of dissolved components (analysts E.N. Perova and A.I. Brusnitsyn).

RESULTS AND DISCUSSION

Assemblage, Morphology, and Anatomy of Phosphates

The primary hydrothermal barite–lead ores were mainly composed of calcite, barite, and galena (Brusnitsyn et al., 2022a). The main minerals of oxidized ores are barite, cerussite, minerals of phosphohedyphane–pyromorphite series, quartz, montmorillonite, and kaolinite; secondary minerals are goethite, hematite, illite, manganite, and other Mn oxides (presumably vernadite and coronadite); accessory minerals are acanthite, naumannite, iodargyrite, cinnabar, malachite, and apatite. Relict galena is preserved even in highly altered ores. In addition, relict calcite, rhodochrosite, pyrite, and, much less frequently, schorl, potassium feldspar, albite, chamosite, clinochlore, and rutile are present in weakly oxidized ores (Brusnitsyn et al., 2022b).

The transformation of ores in the oxidation zone begins with dissolution of calcite and formation of quartz (in some places, possibly, opal?) and products of galena oxidation—cerussite and phosphohedyphane. At this stage, the ground ore mass remains massive. With further intensification of hypergenic processes, the leaching of calcite is no longer compensated by the formation of new minerals. As a result, the rock integrity is violated that lead to the development of numerous micro- and macrokarst occurrences—pores, micro- and larger cavities, partially incrusted with cerussite, phosphohedyphane, pyromorphite, barite, and goethite crystals. The same minerals crystallize in the groundmass. Finally, complete dissolution of calcite and disintegration of ores occurs with the formation of loose sandy-clay deposits typical of oxidation zones.

Lead phosphates were found in ores of various degrees of alteration. They are represented by several successively formed minerals, which differ in morphology and anatomy of crystals, as well as in the chemical composition of minerals (Figs. 1–3). At the earliest stages of oxidation, phosphohedyphane crystallizes in ores. It occurs as chemically homogeneous crystals of dipyramidal–prismatic habit of 30 μm long and 10 μm wide (Figs. 1a, 3a). A number of crystals of early phosphohedyphane does not exceed 1–3% of the rock volume, being mostly concentrated in quartz cementing incompletely dissolved calcite grains. Cerussite with galena inclusions and idiomorphic or partially corroded pyrite crystals occur in the same assemblage; rhodochrosite, chamosite, and some other minerals are less common.

Lead phosphates are much more widespread in the later cavities left from dissolution of calcite. Their amount here increases reaching the level of the main minerals (>5 vol %). Due to their bright lettuce-green color they are well recognizable even in the field. Such lead phosphates from dissolution cavities are widely known to mineralogists and collectors as typical "pyromorphite" of the Ushkatyn-III deposit. However, the composition of these minerals is more complex. At this development stage of oxidation zone there is a growth of phosphates with a rhythmic-zonal pattern, determined by Ca and Pb distribution, the chemical composition of which varies from phosphohedyphane to pyromorphite. Zonal phosphate forms kidney-shaped clusters of radial-fibrous spherulites up to 2–3 mm across, as well as irregular intergrowths (microdruses) of well-faceted crystals of 50–300 μm long and 10–80 μm wide (Figs. 2a–2d, 3b, 3c).

The main simple crystal forms are the hexagonal prism $\{10\bar{1}0\}$, a series of hexagonal dipyramids with indices from $\{10\bar{1}1\}$ to $\{1.0.\bar{1}.20\}$, and the pinacoid $\{10\bar{1}0\}$. Combinations of these simple shapes provide the elongated-prismatic or barrel-shaped habit of the crystals (Figs. 1a–1c), which is generally typical of both lead phosphates and other minerals of the apatite supergroup. The prismatic and dipyramidal faces are usually smooth, sometimes with blocky structure with slight displacement of subindividuals relative to each other. At the same time, the sculpture of pinacoidal faces is always uneven due to the occurrence of numerous growth hillocks. In some places, due to uncoordinated rate of growth of prisms, dipyramids, and pinacoid, crystals become boxy in habit, with external faces and partially hollow interior. Cerussite and barite are associated with zonal phosphates; all these minerals are often covered with goethite crusts.

At the late stages of mineral formation, pyromorphite, homogeneous in composition, crystallizes in the same dissolution cavities. It occurs as short columnar crystals with predominance of hexagonal prism faces $\{10\bar{1}0\}$ and pinacoid $\{10\bar{1}0\}$ dominate in area;

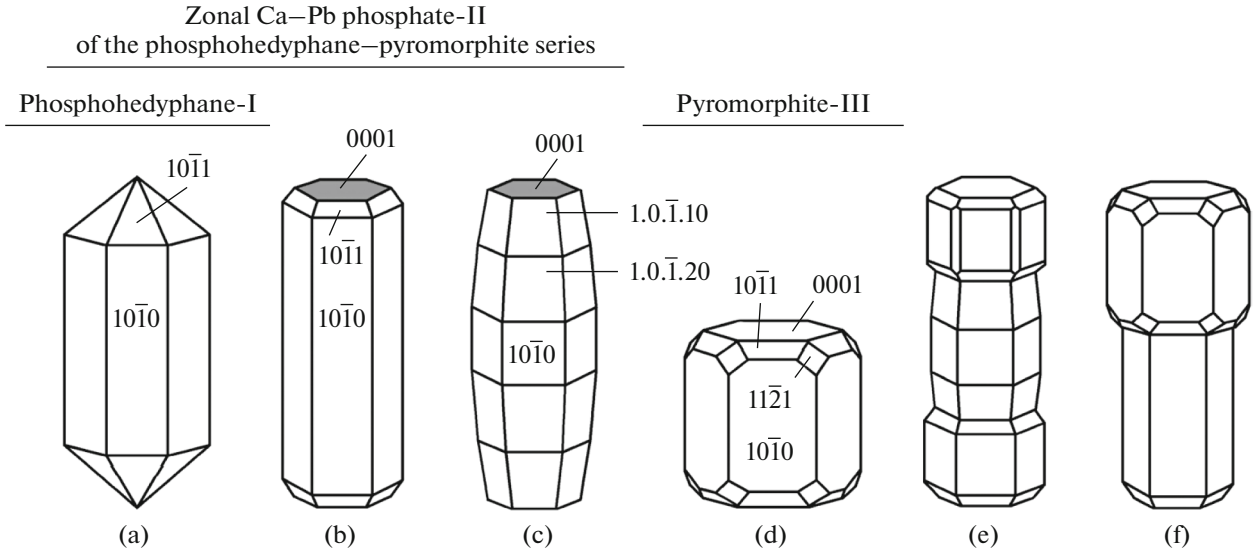

Fig. 1. Idealized morphology of crystals of lead phosphate minerals. The habit of crystals: (a) dipyramidal-prismatic, (b) elongated-prismatic, (c) pinocoidal-pyramidal (barrel-shaped), (d) short-columnar (pinocoidal–prismatic), (e, f) scepter-shaped crystals with short-columnar pyromorphite overgrowing barrel-shaped (e) and elongated-prismatic (f) bases of zonal Ca–Pb phosphate. The planes of the pinacoid, which have an uneven surface formed by numerous tubercles of growth, are shown in gray.

dipyramid faces $\{10\bar{1}1\}$ and $\{1.0\bar{2}.1\}$ are much less developed. Sometimes, such crystals occur as independent individuals, but more often they form scepter-shaped crystals on earlier elongated-prismatic crystals of zonal Ca–Pb phosphate (Figs. 1d–1f, 2d, 2f, 3d).

Thus, in weakly oxidized ores, which still retain massive texture, one can observe the following series of successive lead phosphate formation: (1) dipyramidal-prismatic crystals of chemically homogeneous phosphohedyphane → (2) elongated prismatic and barrel-shaped crystals of zonal phosphate → (3) short columnar crystals of chemically homogeneous pyromorphite. In the first approximation, this series reflects the decrease of Ca content in the mineral-forming medium.

In highly oxidized friable ores, it is extremely difficult to determine the sequence of mineral crystallization. The semiquantitative analysis of phosphates showed the presence of both pyromorphite and phosphohedyphane among them. However, it cannot be said with confidence whether they are formed at late stages of the development of oxidation zone or are inherited from earlier stages.

Chemical Composition of Phosphates

The studied phosphates have a simple chemical composition (Table 1). It was established that these minerals contain only five major elements: O, P, Ca, Pb, and Cl. The contents of other elements are below the detection limit for the EDS detector. Only single analyses yielded trace As impurities (As < 0.10 wt %).

Conversion of the analyses to the typical crystallochemical formula of apatite-supergroup minerals $\left({}^{IX}M1_2^{VII}M2_3\right)_{\Sigma=5}({}^{IV}TO_4)_3X$ shows that the P content in position ${}^{IV}T$ corresponds to the theoretical values P = 2.97–3.02 apfu. Chlorine sharply dominates in anionic position X Cl = 0.83–1.01 apfu, leaving (OH)-groups no more than 0.17 apfu Cationic positions ${}^{IX}M1$ and ${}^{VII}M2$ in different proportions are occupied by calcium and lead. The ratios between the cations vary over a wide range from $(Ca_{1.84}Pb_{3.18})_{\Sigma\,=\,5.02}$ to $(Ca_{0.00}Pb_{4.96})_{\Sigma=4.96}$ (Fig. 4). It is significant that the Ca content does not exceed 2 apfu, while the Pb content does not drop below 3 apfu As in other apatite-supergroup minerals, this is most likely due to the features of cation distribution on two structural positions ^{IX}M1 and ^{VII}M2. The first position is occupied by both Ca and Pb ions, and the second one exclusively by Pb ions (Kampf et al., 2006; Pasero et al., 2010). In such a case, Pb phosphates with Ca > 1 apfu should be assigned to phosphohedyphane, while those with Ca < 1 apfu should be assigned to pyromorphite. Both minerals occur in equal proportions at the Ushkatyn-III deposit. The Ca/Pb ratio in pyromorphite (78% of analyses) are most often in the interval $(Ca_{0.00-0.40}Pb_{4.60-5.00})_{\Sigma\,=\,5.00}$, and the Ca/Pb ratio in phosphohedyphane (69% of analyses) is in that of $(Ca_{1.40-1.70}Pb_{3.30-3.60})_{\Sigma\,=\,5.0}$; other compositions are much rarer. Taking into account the probable distribution of calcium and lead on positions ${}^{IX}M1$ and ${}^{VII}M2$, the median composition of cations in the minerals is as follows: pyromorphite, $[(Ca_{0.22}Pb_{1.78})_{\Sigma\,=\,2.00}Pb_{2.99}]_{\Sigma\,=\,4.99}$, and phosphohedyphane, $[(Ca_{1.48}Pb_{0.52})_{\Sigma=2.00}Pb_{2.99}]_{\Sigma=4.99}$.

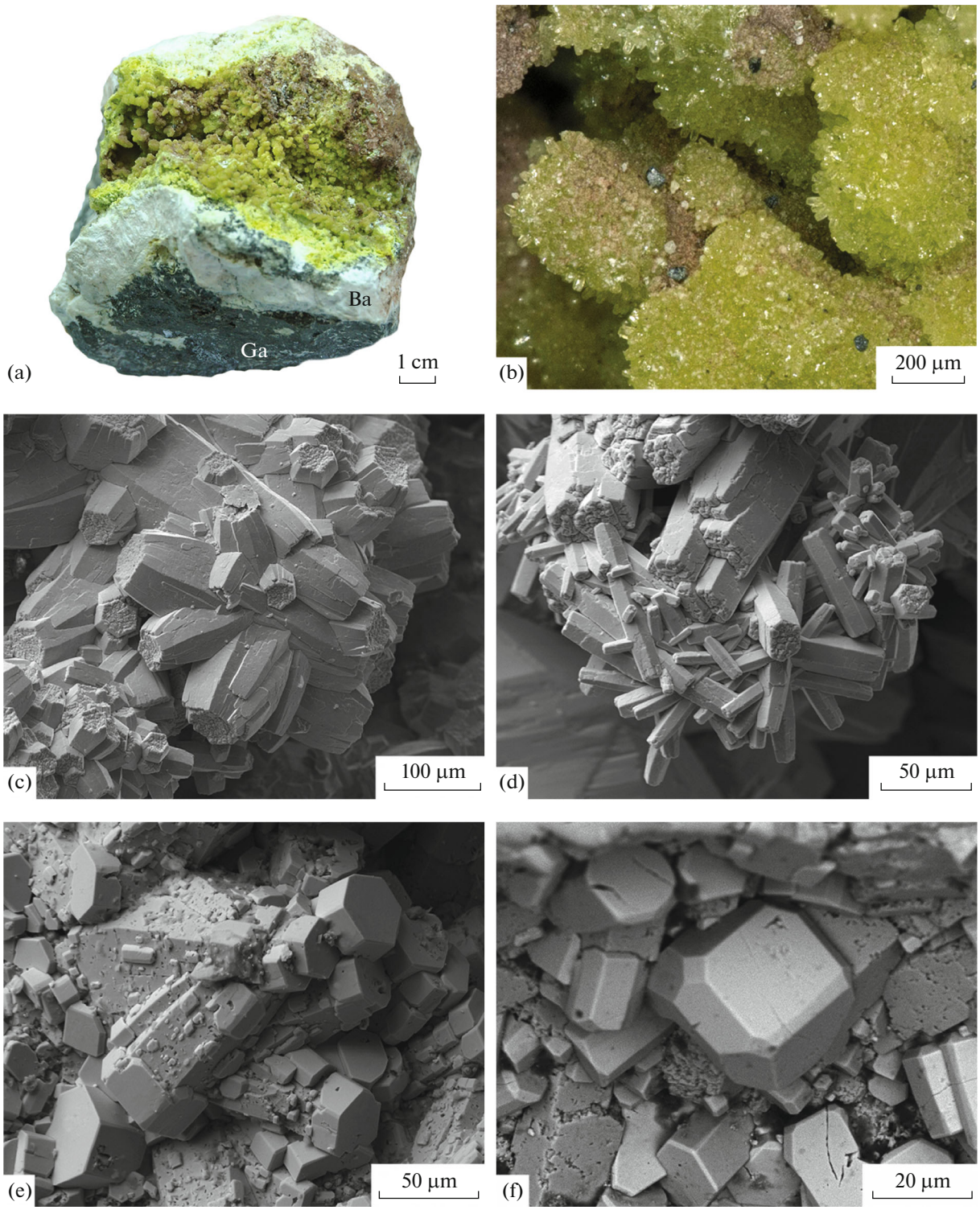

Fig. 2. Morphology of segregations of lead phosphate minerals. Images of samples: (a–b) in reflected light, (c–d) in back-scattered electrons; (a, b) Spherolites and druses of microcrystals of lead phosphate minerals: (a) general view of sample, (b) detail; (c, d) irregular intergrowths (microdruses) of elongated zonal Ca–Pb barrel-shaped phosphates of barrel-shaped (c) and elongated-prismatic (d) habit, sample Ush-409 (it is visible that prism and dipyramid faces are even, pinacoidal ones with tubercles); (e, f) scepter-shaped crystals with short-columnar pyromorphite overgrowing the elongated-prismatic bases of Ca–Pb phosphate, sample Ush-403 (perfectly even faces of pyromorphite, faces of the Ca–Pb phosphate and "micro-cellular," block-structured). Porous segregations in center of Fig. 2f are represented by goethite; Ga—galena, Ba—barite.

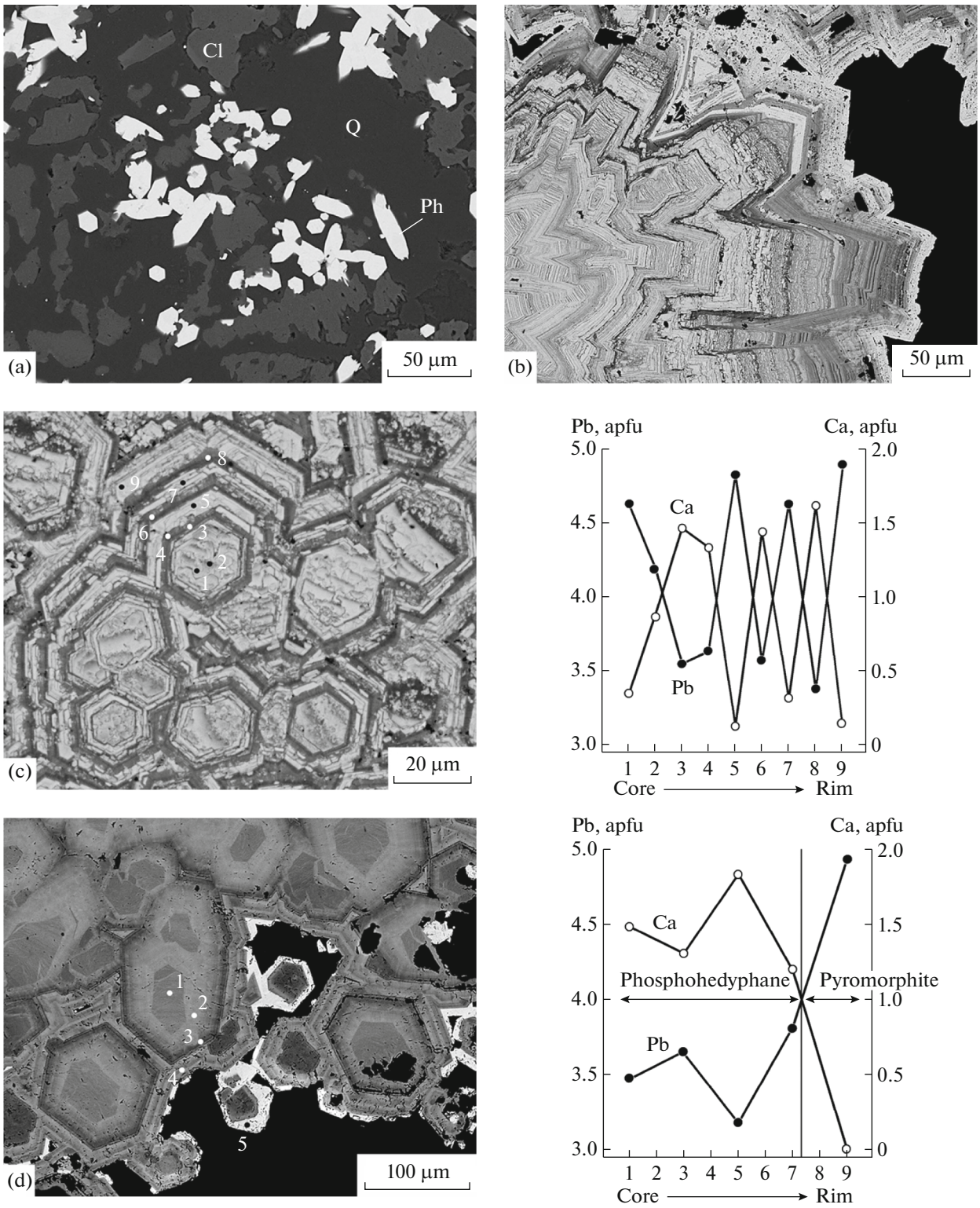

Fig. 3. Anatomy of lead phosphate crystals. BSE images of polished sections: (a) segregations of chemically homogenous dipyramidal-prismatic crystals of phosphohedyphane in quartz replacing calcite; (b) longitudinal section of radial fibrous intergrowths of thinly rhythmically zonal Ca–Pb phosphate crystals; (c, d) cross-sections of zonal Ca–Pb phosphate crystals (c) and of phosphohedyphane with rims of the later pyromorphite (d). In the left, images of samples; on the right, distribution plots of Ca and Pb by zones of crystal growth. Numbers 1–9 on plots correspond to points on images and to numbers of analyses in Table 1. Transition from zones enriched in Pb (light gray) to zones enriched in Ca (dark gray) in images (b–d) is shown in grades of gray color; black spots—cavities. Minerals: Q—quartz, Cl—calcite, Ph—phosphohedyphane; f.c.—crystallochemical coefficients in formulas.

Table 1. Chemical composition (wt %) and coefficients of crystallochemical formulas of phosphates

Component	Numbers of samples														
	Ush-151	Ush-409									Ush-403				
		1	2	3	4	5	6	7	8	9	1	2	3	4	5
P_2O_5	19.50	16.54	17.24	19.20	18.97	16.23	19.14	16.60	19.81	16.11	19.43	18.80	20.06	18.42	15.90
CaO	8.40	1.46	4.05	7.41	6.62	0.56	7.26	1.38	8.43	0.63	7.61	6.51	9.70	5.81	0.00
PbO	69.15	80.17	76.36	71.30	71.71	81.49	71.49	79.87	70.08	82.13	70.54	71.94	66.90	73.34	82.23
Cl	2.96	2.45	2.48	2.80	2.76	2.42	2.78	2.27	2.97	2.33	2.65	3.07	3.31	2.85	2.59
Total	100.01	100.62	100.13	100.71	100.06	100.70	100.67	100.12	101.29	101.20	100.23	100.32	99.97	100.43	100.72
$O=Cl_2$	0.68	0.56	0.57	0.64	0.63	0.56	0.64	0.52	0.68	0.54	0.61	0.71	0.76	0.66	0.60
Total	99.33	100.06	99.56	100.07	99.43	100.14	100.03	99.60	100.61	100.66	99.62	99.61	99.21	99.77	100.12
	Coefficients were calculated per 25 cations														
P	2.98	3.01	2.97	3.00	3.01	3.02	3.00	3.02	3.00	3.00	3.01	3.01	2.99	3.00	3.01
Pb	3.04	2.98	3.07	3.01	2.96	2.95	3.00	2.95	3.00	3.01	2.97	3.66	3.02	3.00	2.96
Total $^{VII}M2$	3.04	2.98	3.07	3.01	2.96	2.95	3.00	2.95	3.00	3.01	2.97	2.98	3.02	3.00	2.96
Pb	0.35	1.66	1.12	0.53	0.67	1.87	0.56	1.68	0.38	1.85	0.51	0.68	0.16	0.80	2.00
Ca	1.65	0.34	0.88	1.47	1.33	0.13	1.44	0.32	1.62	0.15	1.49	1.32	1.84	1.20	0.00
Total $^{IX}M1$	2.00	2.00	2.00	2.00	2.00	2.00	2.00	2.00	2.00	2.00	2.00	2.00	2.00	2.00	2.00
Cl	1.01	0.90	0.87	0.89	0.89	0.91	0.88	0.84	0.91	0.88	0.83	1.00	1.00	0.94	1.00
$(OH)^{calc}$	0.00	0.10	0.13	0.11	0.11	0.09	0.12	0.16	0.09	0.12	0.17	0.00	0.00	0.06	0.00
Total X	1.01	1.00	1.00	1.00	1.00	1.00	1.00	1.00	1.00	1.00	1.00	1.00	1.00	1.00	1.00

The table presents analyses of minerals from weakly oxidized ores: Sample Ush-151—massive rock, phosphohedyphane from quartz, replacing calcite; samples Ush-409 and Ush-403—cavernous rocks: zonal Ca–Pb phosphates from dissolution cavities left from calcite (sample Ush-409, rhythmically zonal crystals with maximum contrast distribution of Ca and Pb by zones of growth; sample Ush-403, zonal phosphohedyphane with (scepter-shaped overgrowing) pyromorphite rim). Numbers of analyses 1–9 and 1–5 correspond to points in Figs 3c and 3d.

The earliest phosphohedyphane from massive calcite-quartz segregations is chemically homogeneous and is characterized by one of the highest Ca contents among the studied phosphates (Table 1, sample Ush-151). The crystallochemical formula of the mineral is written as $[(Ca_{1.65}Pb_{0.35})_{\Sigma\ =\ 2.00}Pb_{3.04}]_{\Sigma\ =\ 5.04}(P_{2.98}O_{12})Cl_{1.01}$.

Elongated-prismatic phosphate crystals from dissolution cavities are always zonal by calcium and lead distribution (Table 1, analyses of samples Ush-409 and Ush-403). The growth zonation is thin-rhythmic oscillatory with frequent alternation of zones contrast in the composition (3–10 μm thick, rarely more). They are sharply enriched either in Pb (Pb $\gg$ 4 apfu, Ca $\ll$ 1 apfu) or calcium (Ca $\gg$ 1 apfu, Pb $\ll$ 4 apfu) (see Figs. 3b and 3c). Second-order finer zonation is often observed within individual zones. There are also cases in which fluctuations in Pb and Ca contents along the growth zones are less sharp. In terms of chemical composition, minerals generally correspond to pyromorphite (Ca < 1 apfu) or phosphohedyphane (Ca > 1 apfu) (see Fig. 3d). There are also specific variants of zonality differing in the thickness of growth zones, their number, variations in composition, etc. This may be due to several reasons. Among them, for example, are different sections of a bulk rock sample in a parallel thin-section, different spatial orientations of crystals, different rates of growth of neighboring crystals or even their separate faces, local variations in physicochemical conditions, etc. Nevertheless, there is a statistically traceable, quite definite tendency to a gradual increase in the Pb content in the outer parts of zonal crystals. An additional confirmation of this trend is the formation of clusters of scepter-shaped crystals, the base of which is represented by zonal crystals and the outer tips of which are represented by chemically homogenous pyromorphite.

Pyromorphite, the latest phosphate, forming short columnar crystals in dissolution cavities, has a homogeneous chemical composition, which is practically the same as the model composition of this mineral (Table 1, analysis 5 of sample Ush-403).

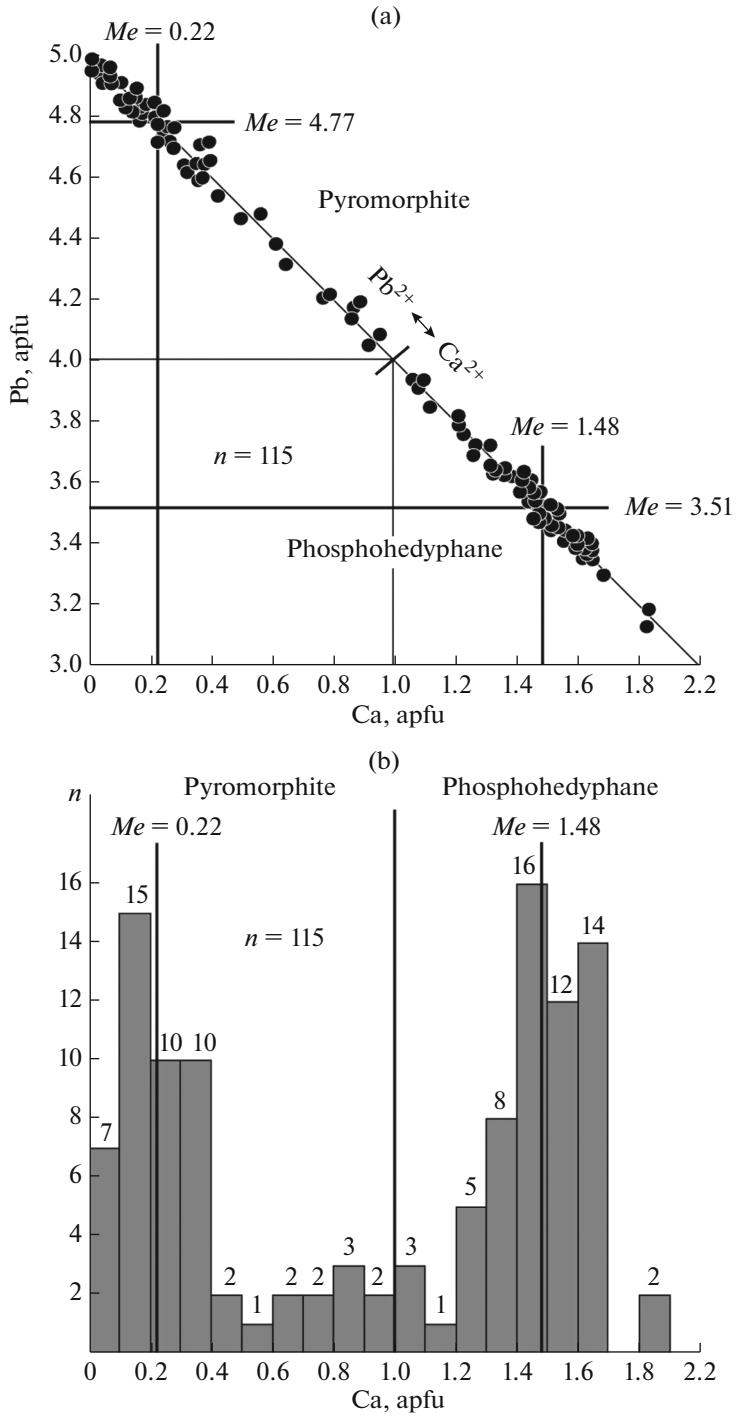

Fig. 4. (a) Distribution of Ca and Pb contents and (b) histogram of calcium contents in lead phosphates minerals. *n*—number of analyses, *Me*—median. Numbers over columns at Fig. 4b—number of analyses.

X-ray Parameters

The diffractograms of all the studied samples are close to the reference data for pyromorphite, "calcic pyromorphite" and phosphohedyphane in position and intensity of peaks (PDF-2 ICDD-2020 nos. 01-075-8296, 01-084-0815, 01-083-3040). The main diagnostic lines are (sample Ush-403, d(Å)/I): 8.51/6, 4/27/18, 4.07/52, 3.61/17, 3.33/16, 3.12/22, 2.95/100, 2.92/57, 2.85/25, 2.41/4, 2.16/11, 2.14/6, 2.04/11, 1.98/7, 1.93/15, 1.89/10, 1.84/10, and 1.81/5.

Most diffractograms show broadening and often splitting of reflexes, which is especially evident begin-

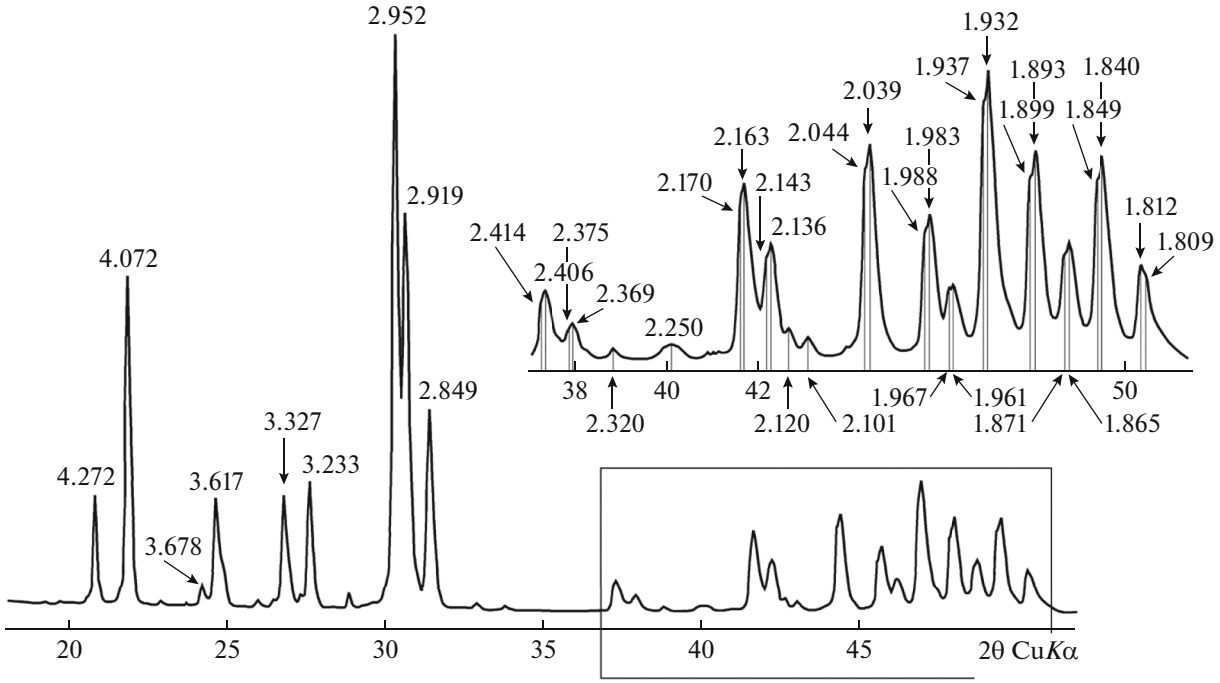

Fig. 5. X-ray diffraction pattern of a zonal Ca–Pb phosphate. Data for the sample Ush-403 where the principal volume of crystals corresponds to phosphohedyphane; a thin outer rim—to pyromorphite. Fraction numbers mark values of interplanar distances of reflections, in angströms.

ning from angles 2Θ = 37° (Fig. 5). Obviously, this is due to the heterogeneity of the chemical composition of the samples being analyzed, variations in Ca and Pb contents in the crystal growth zones, leading to changes in unit cell parameters and, accordingly, the shift of X-ray reflections from the same grids of the crystal lattice (with the same symbols *hkl*).

Hence, it is possible to estimate by the Rietveld method the quantitative ratios of the sites of the same sample varying in chemical composition, as well as the occupancy of structural positions $^{IX}M1$ and $^{VII}M2$ in phosphates by Ca and Pb cations. The latter is especially important for phosphohedyphane, since the predominant concentration of Ca cations in position $^{IX}M1$ (rather than a fundamentally possible uniform distribution of cations of this element between both positions $^{IX}M1$ and $^{VII}M2$) is one of the criteria determining the species affiliation of this mineral. In this connection, the sample Ush-403 was chosen for study due to the main volume of crystals (about 80–90%) corresponds to phosphohedyphane in terms of chemical composition, and the thin outer rim—to pyromorphite. The Ca content in the inner parts of such crystals varies in growth zones, but always exceeds one per crystallochemical formula. In addition, the Ca content in the outer zones is below the detection limit of the EDS detector (see Table 1, Fig. 3d).

The results of X-ray diffraction processing using Rietveld method show that the composition of the sample studied contains approximately equal amounts of two main crystalline phases: phase-1 $a = 9.877(1)$, $c = 7.214(1)$ and phase-2 $a = 9.907(1)$, $c = 7.255(1)$ Å. One of the cationic positions ($^{IX}M1$) in both "phases" is occupied by Pb and Ca ions in the following proportions: phase-1, Pb^{2+} 33%, Ca^{2+} 67%; phase-2, Pb^{2+} 56%, Ca^{2+} 44%; the second cationic position ($^{VII}M2$) is entirely occupied by Pb ions. Taking into account the stoichiometry of phosphates, the calculated distribution of cations by crystallochemical positions is as follows: phase-1 $[(Ca_{1.34}Pb_{0.66})_{\Sigma = 2.00}Pb_{3.00}]_{\Sigma = 5.00}$, phase-2 $[(Ca_{0.88}Pb_{1.12})_{\Sigma = 2.00}Pb_{3.00}]_{\Sigma = 5.00}$.

The data obtained do not fully correspond to the results of chemical analyses. In terms of the crystallochemical formula of minerals, the averaged chemical compositions of the central (volume-dominant) parts of crystals are well correlated with the compositions of phase-1. However, there are no compositions corresponding to phase-2 in the crystals being analyzed. The reasons for this discrepancy are quite understandable, taking into account the thin rhythmic-zonal structure of the crystals. The separate growth zones were studied by point-counter chemical analysis. At the same time, X-ray analysis was applied for a bulk powder sample, the total composition of which does not fully correspond to the totality of single microanalyses. Most likely, this is the reason that the calculated composition of phase-2 is noticeably deviated from the real stoichiometry of the studied phosphates. Apparently, the reflexes attributed to phase-2 characterize thin phosphohedyphane–pyromorphite

intergrowths, which are developed at the boundary between the outer and inner zones of crystals. Clarification of the X-ray parameters of phase-2 requires additional studies, which are difficult to realize using the material available.

The main result of using Rietveld method is the confirmation of the regular distribution of Ca^{2+} and Pb^{2+} cations on two crystallochemical positions $^{IX}M1$ and $^{VII}M2$. Moreover, the assumptions made earlier on the basis of interpretation of analytical chemical data and general ideas about crystal structure of Ca–Pb phosphates are additionally substantiated in an independent way. Thus, the attribution of minerals with Ca > 1 apfu and Ca < 1 apfu to phosphohedyphane and pyromorphite, respectively, is quite in order for the Ushkatyn-III deposit.

GENETIC INTERPRETATION

The conditions of lead mineral formation in subsurface settings have been actively studied by experimental and computational methods to solve both geologic and environmental issues (Garrels and Christ, 1965; Nriagu, 1974, 1984; Manecki et al., 2000, 2020; Miretzky, Fernandez-Cirelli, 2008; Brookins, 2011; Burmann et al., 2013; Markl et al., 2014; Keim and Markl, 2015; Ondrejka et al., 2020; Li et al., 2021, 2022). The results of the above works, together with the original calculations of phase equilibria, help one to interpret the obtained mineralogical observations in a more correct way. At the same time, when studying phosphates, we have to be guided by the data on pyromorphite, since experimental studies of phosphogediphane stability have not been carried out yet, and, accordingly, the values of thermodynamic constants for this mineral have not been determined.

At the Ushkatyn-III deposit, the key mineralogical transformations of initially hydrothermal barite–lead ores under the influence of surface meteoric waters are dissolution of calcite and development of cerussite and lead phosphates after galena, while barite remains stable. Let us consider these processes from the point of view of chemical reactions.

The development of cerussite after calcite-galena assemblage may be conveniently represented schematically as a reaction (Brusnitsyn et al., 2022b):

$$n\mathrm{CaCO_3} + \mathrm{PbS} + (n-1)\,\mathrm{H^+} + 2\mathrm{O_2} = \mathrm{PbCO_3} + n\mathrm{Ca^{2+}} + \mathrm{SO_4^{2-}} + (n-1)\,\mathrm{HCO_3^{2-}}.$$

According to this equation, the carbon dioxide released during dissolution of calcite is partly concentrated in lead carbonate and partly enters the solution. Calcium and sulfate ion also enter the solution. Lead is preserved in the system, being fixed in the form of hardly soluble cerussite. Physicochemical calculations show that cerussite can crystallize under a wide range of pH conditions in an oxidizing environment under relatively high CO_2 concentrations in solution. For example, cerussite is stable at pH from 5.5 to 9.5 at a dissolved lead activity of 10^{-6} and CO_2 activity of 10^{-2}, i.e., in the range covering the compositions of almost any groundwater (Fig. 6a). Cerussite is stable both in assemblage with calcite (at pH ≥ 8) and in more acidic media, when calcite is already completely dissolved.

The crystallization of lead phosphates occurs under actually the same conditions as the formation of cerussite. In the case of the presence of phosphorus and chlorine in solution, pyromorphite is stable over a very large range of redox and acid–alkali conditions (Nriagu, 1974, 1984). The stability field of pyromorphite is located in the central part of Eh–pH diagrams. The left boundary of its stability field on the side of acidic media (pH ≈ 5) is determined by the reaction

$$\mathrm{Pb_5(PO_4)_3Cl} + 6\mathrm{H^+} = 5\mathrm{Pb^{2+}} + 3\mathrm{H_2PO_4^-} + \mathrm{Cl^-}.$$

The decrease of acidity (for example, due to dissolution of calcite) will shift this equilibrium to the left, towards the formation of phosphate. The right boundary on the side of alkaline media is controlled by the following reaction:

$$\mathrm{Pb_5(PO_4)_3Cl} + 15\mathrm{H_2O} = 5\mathrm{Pb(OH)_3^-} + 3\mathrm{HPO_4^{2-}} + \mathrm{Cl^-} + 12\mathrm{H^+}.$$

However, its realization in nature is extremely unlikely, since CO_2 is always present in groundwater, especially at the contact with carbonates. Due to this, pyromorphite is not dissolved under alkaline conditions, but replaced by lead carbonates: at low activity of carbonic acid, by hydrocerussite; at higher activity, by cerussite. This fact determines the possibility of coexistence of pyromorphite with cerussite:

$$\mathrm{Pb_5(PO_4)_3Cl} + 5\mathrm{HCO_3^-} = 5\mathrm{PbCO_3} + 3\mathrm{HPO_4^{2-}} + \mathrm{Cl^-} + 2\mathrm{H^+}.$$

The position of the pyromorphite–cerussite equilibrium line depends on the solution composition. Increasing concentrations of phosphate-ion and/or chlorine widens the stability field of pyromorphite and shifts its boundary to the right toward higher pH values, thus reducing the stability field of cerussite. On the contrary, increasing the CO_2 concentration narrows the stability field of pyromorphite, but expands that of cerussite. Accordingly, the boundary of the stability fields of these minerals shifts to the left, toward lower pH values. Figure 6b presents a variant of the Eh–pH diagram, where the boundary of the stability fields of pyromorphite and cerussite is located near pH ≈ 8–8.5 and where the processes of dissolution/deposition of calcite in subsurface conditions occur. Apparently, these are the conditions that constrain the coexistence of pyromorphite and cerussite in the ores being studied.

Stability of pyromorphite in a wide range of acid–alkaline and redox conditions determine the possibil-

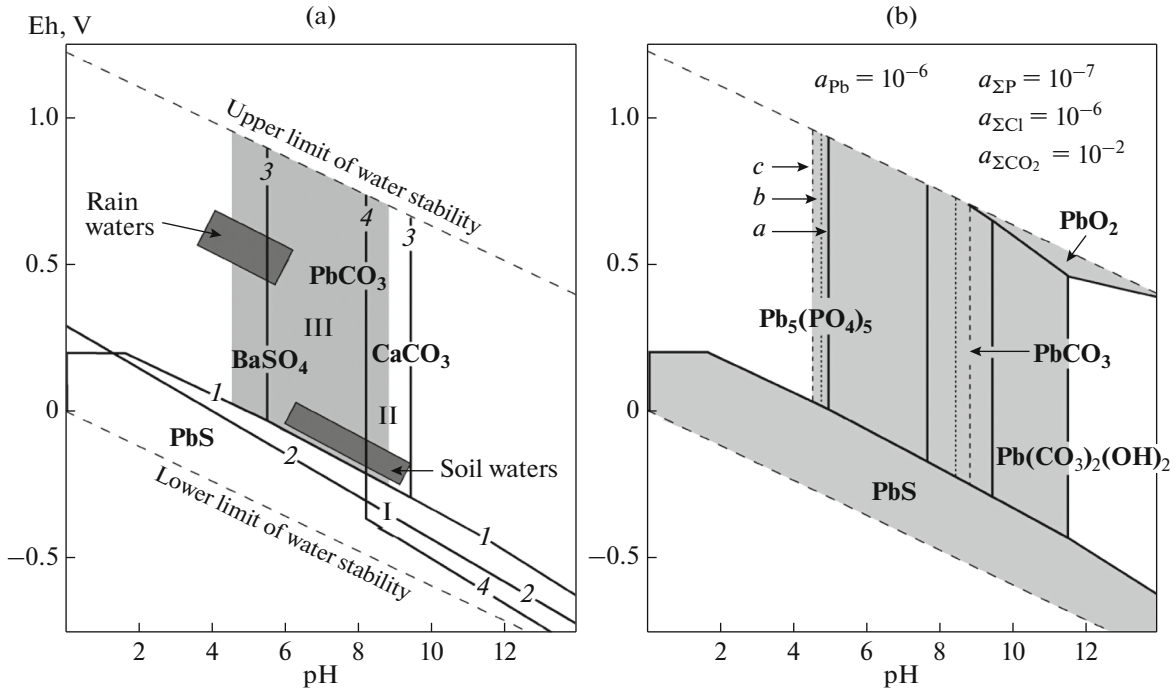

Fig. 6. Eh–pH diagrams of stability of minerals in water at 25°C and 1 bar: (a) for galena, cerussite, barite, calcite, and pyromorphite (Brusnitsyn et al., 2022b, with amendments); (b) for lead minerals. In Fig. 6a, numbers mark boundaries delineating stability fields for (*1*) galena, (*2*) barite, (*3*) cerussite, and (*4*) calcite. Roman numerals mark stability fields for mineral assemblages of primary hydrothermal ores (I): calcite + galena + barite; weakly oxidized ores (II): calcite + cerussite + barite; strongly oxidized ores (III): cerussite + barite. The light-gray area shows the field of pyromorphite stability (the largest field in Fig. 6b); fields of Eh–pH parameters of rain and ground waters are shown by dark-grey rectangles. The diagram was constructed for the following conditions: activity of dissolved Pb and Ba—10^{-6}, Ca—10^{-4}, general activity of dissolved S and C compounds—10^{-2}. In Fig. 6b, the fields of stability of solid phases are shown in grey, (*a*) thick continuous lines show boundaries of stability of minerals under conditions shown on the figure, thin dotted lines—under the following conditions: (*b*) general activity of dissolved phosphorus compounds—10^{-7}, chlorine—10^{-4}, (*c*) general activity of dissolved phosphorus compounds—10^{-6}, chlorine—10^{-6}. In all cases general activity of dissolved sulfur compounds—10^{-2}. Minerals*:* PbS—galena, PbO_2—plattnerite, $PbCO_3$—cerussite, $Pb_3(CO_3)_2(OH)_2$—hydrocerussite, $CaCO_3$—calcite, $BaSO_4$—barite, $Pb_5(PO_4)_3Cl$—pyromorphite.

ity of its coexistence with minerals slightly affected by alteration of ores in the subsurface setting (in the Ushkatyn-III deposit: with galena, pyrite, barite, calcite, rhodochrosite, cerussite, chamosite, etc.) and with minerals of highly oxidized ores (cerussite, montmorillonite, kaolinite, goethite, etc.).

The formation of lead phosphates does not require large P and Cl concentrations in solution. The solubility products of pyromorphite-series minerals are estimated to be extremely low: $K_{sp} = n \times 10^{-77}$ for hydroxyl–pyromorphite $Pb_5(PO_4)_3(OH)$, and $K_{sp} = n \times 10^{-84}$ for pyromorphite $Pb_5(PO_4)_3Cl$ (Nriagu, 1984; Miretzky and Fernandez-Cirelli, 2008: Lurie, 2012; Li et al., 2022). Therefore, even negligibly low Pb, P, and Cl contents in solution can lead to the crystallization of pyromorphite. Moreover, until the exhaustion of dissolved phosphorus and chlorine, lead will be concentrated in the composition of pyromorphite, and not, for example, cerussite, the solubility product of which is seven orders of magnitude (!) greater (K_{sp} ($PbCO_3$) = 8×10^{-14} (Nriagu, 1984; Lurie, 2012; Li et al., 2022)).

Chlorine is one of the most typical anions in groundwater of different composition and origin (Brownlow, 1984; Linder, 1986; Zverev, 2007). However, there are several possible sources of phosphorus: (1) xenogenic "nonorganic" apatite, which is present in the primary ores and host limestones as part of debris from metamorphic and igneous rocks surrounding the deposit area, (2) authigenic "organic" apatite formed in the course of diagenesis of biogenic phosphate matter accumulated in the form of dead microorganisms during the carbonate sedimentation, and (3) phosphate-ion extracted by meteoric waters from the organic matter of the soil cover overlying the ore deposits.

The last variant seems to be the most probable. Apatite is an accessory mineral in nonoxidized barite–lead ores and host limestones. Its amount is much less than 1% of the rock volume, which is obviously insufficient for formation of phosphohedyphane and pyromorphite in oxidized ores, the contents of which in some places reaches the contents of rock-forming minerals. In addition, according to the data of AO Zhairemsky GOK (2015), the average P content in

oxidized ores is almost 20 times higher than that in the primary ores (Brusnitsyn et al., 2022b). Such a large increase in P content is difficult to explain only as a result of complete dissolution of calcite and, consequently, an increase in the concentration of all other components in oxidized ores. For example, the Pb, Ba, and Si contents in the oxidized ore increase on average by about two times. compared to those in the primary ore. In turn, the Ti, Al, and Fe contents increase by about three, five, and six times, respectively. Against the background of these values, the increase in P content appears to be anomalously high. It is most reasonable to attribute it to additional P input from external sources.

Nevertheless, the formation of a small part of lead phosphates due to apatite contained in the initial ores cannot be completely excluded. The solubility products of hydroxyl–apatite K_{sp} ($Ca_5(PO_4)_3(OH) = n \times 10^{-58}$ and fluoroapatite K_{sp} ($Ca_5(PO_4)_3F = n \times 10^{-28}$ are many orders of magnitude greater than those of pyromorphite (Miretzky and Fernandez-Cirelli, 2008; Lurie, 2012). Consequently, apatite becomes unstable in the presence of lead ions in solution (resulting from dissolution of galena) and will be replaced by pyromorphite:

$$Ca_5(PO_4)_3(OH) + 5Pb^{2+} + Cl^- + H^+ = Pb_5(PO_4)_3Cl + 5Ca^{2+} + H_2O.$$

However, crystallization of the bulk of lead phosphate is most likely due to biogenic phosphate ion brought into the ores by meteoric waters penetrating through the soil cover. This has been proved for a large number of deposits by analyzing the oxygen isotope composition of pyromorphite (Burmann et al., 2013). In this case, pyromorphite can be crystallized either directly from solution or formed by replacement of previously formed cerussite. The corresponding reactions have been summarized above.

The presence of calcium in the mineral-forming environment has markedly affected the chemical compositions of phosphates, which evolve in time from extremely Ca-rich phosphohedyphane through intermediate Ca–Pb minerals of the phosphohedyphane–pyromorphite series to nearly Ca-free pyromorphite. Such a general trend reflects a gradual decrease in Ca content in solution as weathering processes develops, accompanied by depletion in calcite (the main Ca source) and dilution of pore solutions by new portions of meteoric waters. However, the trend in the change in solution composition was not linear: slight fluctuations in Ca content occurred periodically against the general regressive background, and, as long as this element remained in solution, it "competed" with lead for a position in the crystal structure of phosphate. As a result, phosphates zonal in composition crystallized. Moreover, the development of zonality can be caused by different reasons, both external ones with respect to the sites of mineral formation and internal ones associated with the mechanism of crystal growth under relatively stable external conditions. Among the first reasons, for example, are seasonal variations in groundwater composition, which is generally characteristic of subsurface environments. Among the second ones are "pulsating" change in supersaturation with some elements (in our case, Ca and/or Pb) at the front of crystal faces growth from solutions heterogeneous in the chemical composition. A regular "discharge" of such local supersaturation due to the capture of the corresponding elements by the mineral leads to the formation of oscillation zonality (Grigoriev and Zhabin, 1975; Krasnova and Petrov, 1997).

It is interesting to emphasize two more features. First, the widespread development of zonal phosphate crystals with contrasting separation of elements in growth zones and well-defined grouping of chemical compositions around two extrema with calcium contents of 0.22 and 1.48 apfu, respectively, may reflect incomplete miscibility of lead and calcium in the isomorphic series phosphohedyphane $Ca_2Pb_3(PO_4)_3Cl$–pyromorphite $Pb_2Pb_3(PO_4)_3Cl$. Second, the Ca content in phosphohedyphane from the Ushkatyn-III deposit does not exceed 2 apfu even if this mineral is closely associated with calcite bearing distinct traces of dissolution. Obviously, the composition of the mineral was determined in this case not only by the composition of the Ca- and Pb-rich mother solution, but also by crystallochemical factors that allow calcium cations to enter only in position $^{IX}M1$ of phosphates. Indirectly, this confirms the hypothesis of previous researchers (Kampf et al., 2006) that there is a $Ca^{2+} \leftrightarrow Pb^{2+}$ miscibility gap in the phosphohedyphane $Ca_2Pb_3(PO_4)_3Cl$–Cl–apatite $Ca_2Ca_3(PO_4)_3Cl$ series under low temperatures.

However, it should be noted that phosphohedyphane with Ca content up to 2.46 apfu and its (OH)-group-rich variety (potentially a new mineral species with (OH) > Cl) with Ca content up to 2.74 apfu are still known in nature (Ondrejka et al., 2020).

CONCLUSIONS

The main results of the studies that have been performed are as follows.

(1) Ca–Pb phosphates corresponding to phosphohedyphane and pyromorphite in chemical composition occur equally frequently in the oxidation zone of barite–lead ores of the Ushkatyn-III deposit.

(2) As the ore oxidation processes develop, compositions of newly formed phosphates change regularly in the sequence phosphohedyphane → rhythmic-zonal Ca–Pb phosphate → pyromorphite. At the same time, the habit of phosphate crystals changes from dipyramidal–prismatic through elongated prismatic (barrel-shaped) to pinacoidal–prismatic (short columnar).

(3) Pyromorphite (and most likely, phosphohedyphane) is stable under a wide range of alkali–acid and redox conditions. Lead phosphates can coexist both with minerals almost nonaltered (galena, pyrite, barite, calcite, rhodochrosite, cerussite, chamosite, etc.) and with minerals of highly oxidized ores (cerussite, montmorillonite, kaolinite, goethite, etc.).

(4) Crystallization of pyromorphite is possible already at very low Pb, P, and Cl contents in solution. The main sources of chlorine are groundwater, and those of phosphorus are organic matter of overlying ore-bearing deposits of the soil cover.

(5) The features of chemical composition and crystalline structure of Ca–Pb phosphates, as well as the character of their assemblages allow us to suggest that there is a break of isomorphic miscibility in the pyromorphite—phosphohedyphane and phosphohedyphane—chloroapatite series.

ACKNOWLEDGMENTS

We are grateful to A.Y. Burkovsky, Chairman of the Board of AO Zhairemsky GOK (village of Zhairem, Republic of Kazakhstan) and geologists of this enterprise V.A. Volkov, O.A. Muratov, A.N. Abdelmanova, J.J. Akimeev, K.A. Akshalova, A.S. Burkhanov, R.B. Ivakova, and G.K. Turlynova for assistance in the realization of fieldwork.

FUNDING

The research was carried out using analytical capabilities of the St. Petersburg State University resource centers "X-ray Diffraction Methods of Research," "Microscopy and Microanalysis," and "Geomodel."

CONFLICT OF INTEREST

The authors of this work declare that they have no conflicts of interest.

REFERENCES

Atlas of Mineral Deposit Models of the Republic of Kazakhstan, Daukeev, S.Zh., Uzhkenov, B.S., Bespaev, Kh.A., Miroshnichenko, L.A., Mazurov, A.K., Sayduakasov, M.A., Eds., Almaty: Center Geoinformation MF RK, 2004.

Bethke, C.M., *Geochemical Reaction Modeling,* New York: Oxford University Press Inc., 1996.

Birch, W.D. and Mills, S.J., Sulphide–carbonate reaction in recrystallised limestone at Lilydale, Victoria, Australia: a new occurrence of phosphohedyphane, *Austral. J. Miner.*, 2007, vol. 13, pp. 73–82.

Brownlow, A.H., *Geochemistry,* London: Prentice-Hall Inc., 1979.

Brookins, D.G., *Eh–pH Diagrams for Geochemistry,* New York: Springer, 2011.

Brusnitsyn, A.I., Perova, E.N., Vereshchagin, O.S., Britvin, S.N., Platonova, N.V., and Shilovskikh, V.V., The mineralogy of iron and manganese ores of the Ushkatyn-III deposit in Central Kazakhstan, *Geol. Ore Deposits,* 2021a, vol. 63, No. 8, pp. 772–792.

Brusnitsyn, A.I., Perova E.N., Vereshchagin, O.S., and Vetrova, M.N., Geochemical features and accumulation conditions of Mn-bearing sediments in the complex (Fe–Mn and $BaSO_4$–Pb) Ushkatyn-III deposit, Central Kazakhstan, *Geochem. Int.,* 2021b, vol. 59, no. 9, pp. 858–888.

Brusnitsyn, A.I., Sadykov, S.A., Perova, E.N., and Vereshchagin, O.S., Genesis of barite–galena ores at the Ushkatyn-III deposit, Central Kazakhstan: analysis of geological, mineralogical, and isotopic ($\delta^{34}S$, $\delta^{13}C$, $\delta^{18}O$) data, *Geol. Ore Deposits,* 2022a, vol. 63, no. 3, pp. 1–21.

Brusnitsyn, A.I., Perova, E.N., Loginov, E.S., Platonova, N.V., Panova, L.A., Vereshchagin O.S., and Britvin, S.N., Mineralogy and genesis of the oxidation zone of barite–lead ores of the Ushkatyn-III deposit, Central Kazakhstan, *Zap. Ross. Mineral. O-va,* 2022b, no. 5, pp. 1–27.

Burmann, F., Keim, M.F., Oelmann, Y., Teiber, H., Marks, M.A.W., and Markl, G., The source of phosphate in the oxidation zone of ore deposits: Evidence from oxygen isotope ompositions of pyromorphite, *Geochim. Cosmochim. Acta*, 2013, vol. 123, pp. 427–439.

Buzmakov, E.I., Shibrik, V.I., Rozhnov, A.A., Sereda, V.Ya., and Radchenko, N.M., Stratiform ferromanganese and base metal deposits in the Ushkatyn ore field (Central Kazakhstan), *Geol. Rudn. Mestorozhd.,* 1975, no. 1, pp. 32–46.

Garrels, R.M. and Christ, C.L., *Solutions, Minerals, and Equilibria,* New York: Harper and Row, 1965.

Grigoriev, D.P. and Zhabin, A.G., *Ontogeniya Mineralov* (Ontogeny of Minerals), Moscow: Nauka, 1975.

Hausmann, J.F.L., *Handbbuch der Mineralogie,* Gottingen: Vandenhoek und Ruprecht, Bd., 1813, pp. 1090–1096.

Jirasek, J., Matysek, D., and Minařiková, A., Phosphohedyphane from the abandoned iron deposit Hranična (Silesia, Czech Republic), *Bull. Mineral. Petrolog.*, 2020, vol. 28, pp. 2570–7345.).
https://doi.org/10.46861/bmp.28.044

Kalinin, V.V., Complex ferromanganese and zinc-lead-barite ores in the Ushkatyn group deposits (Central Kazakhstan), *Vulkanogenno-osadochnye i gidrotermal'nye margantsevye mestorozhdeniya* (Volcanosedimentary and Hydrothermal Manganese Deposits), Vitovskaya, I.V, Eds., Moscow: Nauka, 1985, pp. 5–64.

Kampf, A.R., Steele, I.M., and Jenkins, R.A., Phosphohedyphane, $Ca_2Pb_3(PO_4)_3Cl$, the phosphate analog of hedyphane: Description and crystal structure, *Am. Mineral.,* 2006, vol. 91. P. 1909–1917.

Kayupova, M.M., *Mineralogiya zheleznykh i margantsevykh rud Zapadnogo Atasu (Tsentral'nyi Kazakhstan)* (Mineralogy of Iron and Manganese Ores in Western Atasu (Tsentral'nyi Kazakhstan)), Alma-Ata: Nauka, 1974.

Keim, M.F. and Markl, G., Weathering of galena: Mineralogical processes, hydrogeochemical fluid path modeling, and estimation of the growth rate of pyromorphit. *Am. Mineral.,* 2015, vol. 100, pp. 1584–1594

Krasnova, N.I. and Petrov, T.G., *Genezis mineral'nykh individov i agregatov* (Genesis of Mineral Individuals and Aggregates), St. Petersburg: Nevskii kur'er, 1997.

Leeder, M.R., *Sedimentology. Process and Product,* London: George Allen & Unwin, 1982.

Li, J., Tian, X., Bai, R., Xiao, X., Yang, F., and Zhao, F., Transforming cerussite to pyromorphite by immobilizing Pb(II) using hydroxyapatite and *Pseudomonas rhodesiae, Chemosphere*, 2022, vol. 287, paper no. 132235.

Li, X., Azimzadeh, B., Martinez, C.E., and McBride, M.B., Pb Mineral precipitation in solutions of sulfate, carbonate and phosphate: measured and modeled Pb solubility and Pb^{2+} activity, *Minerals*, 2021, vol. 11, p. 620.

Lur'e, Yu.Yu., *Spravochnik po analiticheskoi khimii* (Reference Book on Analytical Chemistry) Moscow: Kniga po trebovaniyu, 2012.

Manecki, M., Maurice, P.A., and Traina, S.J., Kinetic of aquous Pb reaction with apatites, *Soil Science,* 2000, vol. 165, no. 12, pp. 920–933.

Manecki, M., Kwasniak-Kominek, M., Majka, J.M., and Rakovan, J., Model of interface-coupled dissolution precipitation mechanism of pseudomorphic replacement reaction in aqueous solutions based on the system of cerussite $PbCO_3$—pyromorphite $Pb_5(PO_4)_3Cl$, *Geochim. Cosmochim. Acta,* 2020, vol. 289, pp. 1–13.

Markl G., Marks M.A.W., Holzapfel J., and Wenzel T., Major, minor, and trace element composition of pyromorphite-group minerals as recorder of supergene weathering processes from the Schwarzwald mining district, SW German, *Am. Mineral.,* 2014, vol. 99, pp. 1133–1146.

Miyake, M., Ishigaki, K., and Suzuki, T., Structure refinements of Pb^{2+} ion-exchanged apatites by X-ray powder pattern-fitting, *J. Solid State Chem.,* 1986, vol. 61, pp. 203–235.

Miretzky, P. and Fernandez-Cirelli, A., Phosphates for Pb immobilization in soils: a review, *Environ. Chem. Lett.,* 2008, vol. 6, pp. 121–133.

Mitryaeva, N.M., *Mineralogiya barito-tsinkovo-svintsovykh rud mestorozhdenii Atasuiskogo raiona* (Mineralogy of Barite–Zinc–Lead Ores in Deposits of the Atasu Region), Alma-Ata: Nauka, 1979.

Nriagu, J.O., Lead ortophoshates–IV: Formation and stability in the environment, *Geochim. Cismochim. Acta,* 1974, vol. 38, pp. 887–898.

Nriagu, J.O., Formation and stability of base metal phoshates in soil and sediments, In: *Phosphate Minerals,* Nriagu, J.O. and Moore, P.B., Eds., Berlin: Springer, 1984, pp. 318–329.

Ondrejka, M., Bacik, P., Putis, M., Uher, P., Mikus, T., Luptakova, J., Ferenc, S., and Smirnov, A., Carbonate-bearing phosphohedyphane–"hydroxylphosphohedyphane" and cerussite: supergene products of galwna alteration in Permian aplite (Western Carpathians, Slovakia), *Can. Mineral.,* 2020, vol. 58, pp. 347–365.

Pasero, M., Kampf, A.R., Ferraris, C., Pekov, I.V., Rakovan, J., and White, T.J., Nomenclature of the apatite supergroup minerals, *Eur. J. Mineral.,* 2010, vol. 22, pp. 163–179.

Rozhnov, A.A., Comparative characteristics of manganese deposits of the Atasuysky and Nikopol-chiatursky types, *Geologiya i geokhimiya margantsa* (Geology and Geochemistry of Manganese), Varentsov, I.M, Eds., Moscow: Nauka, 1982, pp. 116–121

Skripchenko, N.S., *Prognozirovanie mestorozhdenii tsvetnykh metallov v osadochnykh porodakh* (Prediction of Non-Ferrous Metal Deposits in Sedimentary Rocks), Moscow: Nedra, 1989.

Varentsov, I.M., Veimarn, A.B., Rozhnov, A.A., Shibrik, V.I., and Soklova, A.L., Geochemical model of the formation of manganese ores in the Famennian riftogenic basin in Kazakhstan (main components, rare earth and trace elements), *Litol. Polezn. Iskop.,* 1993, no. 3, pp. 56–79.

Zhayremskii GOK (Mining and Processing Plant). Annual Report for 2015, AO ZhGOK: 2015.

Zverev, V.P., *Podzemnye vody zemnoi kory i geologicheskie protsessy* (Underground Waters of the Earth's Crust and Geological Processes), Moscow: Nauchnyi mir, 2007.

Translated by D. Voroshchuk